Bucciarelli A., Pal R.K., Maniglio D., Quaranta A., Mulloni V., Motta A., Yadavalli V.K.
Fabrication of Nanoscale Patternable Films of Silk Fibroin Using Benign Solvents, Macromolecular Materials and Engineering, 302 (7), 1700110, 2017
10.1002/mame.201700110

Fabrication of nanoscale patternable films of silk fibroin using benign solvents

Alessio Bucciarelli,[a] Ramendra K. Pal,[b] Devid Maniglio,[a] Alberto Quaranta,[a] Viviana Mulloni,[c] Antonella Motta,[a] Vamsi K. Yadavalli [b,†]

[a] Department of Industrial Engineering, University of Trento, Via Sommarive 9, 38123-Povo (TN), Italy.

[b] Department of Chemical and Life Science, Virginia Commonwealth University, 601 West Main St., Richmond, Virginia 23284-3028, USA.

[c] MicroSystems Technology Research Unit, Fondazione Bruno Kessler, Via Sommarive 18, 38123-Povo (TN).

† Corresponding author E-mail: vyadavalli@vcu.edu

Abstract

The silk protein fibroin is a wondrous biopolymer widely used to form structures that interface with biological entities. In addition to tissue scaffolds, sponges, and films, biochemically modified fibroins can be used in conjunction with techniques such as photolithography and soft lithography to expand their repertoire for micro and nano-fabricated systems. To date, the use of hexafluoro-2-isopropanol (HFIP) has been prevalent as a solvent for fibroin and fibroin "resists". However, high volatility, toxicity, cost, and need for specialized disposal, render the necessity for alternative solvents. In addition, for many applications such as in optics and bioelectronics, smooth, thin (~100 nm and below) fibroin films are a prerequisite, which are not easily achieved using HFIP. Here, we present the use of formic acid (FA) as a sustainable solvent for silk fibroin and fibroin "resist" materials, specifically for micro and nanoscale applications. We demonstrate the reproducible formation and characterization of stable thin films of high homogeneity, smoothness and optical transparency. Critically, these films can then be used for high-resolution photopatterning of proteins using benchtop lithographic techniques. The present study indicates that FA is a relatively benign and more optimal solvent than HFIP for forming smooth, fibroin thin films, and microscale architectures for the fabrication of next generation silk-based optical devices.

Keywords: Silk fibroin, photolithography, thin films, microfabrication, green solvent

1. Introduction

Over the last two decades, the protein fibroin from silkworms has attracted the attention of the materials science community due to its remarkable intrinsic properties. Silk fibroin can be easily processed to obtain a wide range of morphologies including micro-particles, micro-needles, hydrogels, mats, membranes, sponges, and films.[1-5] According to their desired application, the obtained materials can be tuned to display remarkable optical, mechanical, and biological properties. For these reasons, silk fibroin has become one of the most widely used materials for the development of biocompatible scaffolds and devices.[6-12] In addition to macroscale structures, the possibility of creating precise patterns at the micro and nanoscales has opened up fundamental and applied applications in optical devices and bioelectronics.[13] For example, nanopatterns of fibroin can ensure the interaction with light via features on the same order of magnitude as the wavelength of light.[14] Different techniques have been used in order to obtain such micro/nanometer scale silk fibroin architectures. These include nanoimprinting,[14] soft lithography,[15] silk transfer applied micropatterning (STAMP),[16] electron-beam lithography (EBL),[17] breath figures,[18] laser ablation,[19] and photolithography.[20, 21] However, the formation of engineered structures of fibroin with controllable dimensions across multiple length scales, in a high throughput, and environmentally friendly manner continues to be an ongoing challenge.

Photolithography is a highly efficient and cost-effective technique of choice to etch patterns on flat substrates at high resolution and speed. Using photolithography, silk features with a resolution of 50 μm were demonstrated using riboflavin as a photoinitiator in a water-based fibroin solution.[20] Feature resolution closer to 1 μm was obtained by biochemically modifying regenerated fibroin to obtain a photo-crosslinkable fibroin conjugate, which was patterned using UV exposure on a

fibroin film through a photomask.[21] Fibroin films produced by solvent casting solutions have a β-sheet conformation with short range ordered structure,[22-24] responsible for superior physical properties of regenerated fibroin.[25] In most reports to date, both fibroin itself, and the fibroin resist are noted to be insoluble in water. While regenerated silk fibroin (rSF) can be used to form aqueous solutions,[26] it is difficult to achieve highly concentrated and stable aqueous solutions owing to self-assembly induced gelation.[27] Consequently, high resolution processing involving fibroin typically necessitates the use of hexafluoroisopropanol (HFIP) as an organic solvent. However, HFIP is not an optimal solvent owing to its acute oral, dermal and inhalation toxicity, high cost and need for careful disposal.[28] As a fluorinated alcohol, HFIP needs to be handled using the same disposal protocols as pesticides. Further, its high volatility makes it difficult to work with spin coating processes, and to obtain a uniform film thickness.

The use of alternative ("green") solvents for fibroin processing is therefore of great interest, principally for forming stable films, and for micro and nanopatterning. Formic acid (FA) is the simplest organic acid that is also environmentally friendly and easily disposed. While it needs to be handled with similar care, the vapor pressure at 20° C (4.67 kPa) is much lower than that of HFIP (16 kPa), ensuring a slower evaporation. This allows use of this solvent in film deposition that require maintaining a liquid phase for longer times. FA has been previously used alone, or in combination with salt for fibroin dissolution.[29] However to date, no systematic studies have been conducted regarding the possibility of using FA as a solvent for photolithography, and specifically, their use in forming nanoscale films, and micro and nanoscale structures.

In this work, we report on the use of FA as a suitable solvent to form nanoscale films of fibroin as

well as high resolution structures. While thicker (several μm) films of fibroin may be formed using casting,[30] producing thin (100-1000 nm) and ultrathin (1-100 nm) films is challenging.[31] In microelectronics applications involving photoresists, spin coating is a well-known method to produce films with uniform and controlled thickness.[32] For instance, spin coating of fibroin in an ionic liquid was used to form a film with thickness of 480±30nm and surface roughness of 19 nm. A thickness in the range of 10-80 nm was obtained using a spin assisted layer-by-layer process (SA-LbL).[31, 33] Calibration curves for aqueous fibroin solutions showed the dependence between film thickness and spin process parameters (concentration, rpm, time).[13] Most recently, a self-standing membrane of silk nanofibrils with a thickness down to 40 nm was reported.[34] However, these techniques lack the possibility of creating complex patterns/structures following film formation.

Herein, a fibroin protein photoresist is used in combination with spin coating to obtain uniform and stable nanoscale films. Using photolithography, patterning on nanoscale films is demonstrated to obtain precise, high resolution, microscale architectures. We present characterization of the films along with a comparison between films obtained with FA vs. those using HFIP as a solvent. Both solvents result in similar film morphology, roughness and mechanical properties at the nanoscale as observed using atomic force microscopy. However, using spin-coating, FA can form more stable and uniform films with controllable thickness in comparison to HFIP. Given the low cost and environmentally friendly nature of FA, we propose the use of this solvent for high tech applications in using fibroin for optical and bioelectronics applications.

2. Experimental Section

108 **2.1. Synthesis of fibroin photocrosslinkable photoresist**

109 Fibroin extraction from the silk worm (*Bombyx mori*) cocoon was conducted following established
110 protocols.[26] The photocrosslinkable fibroin "photoresist" was synthesized using the method
111 previously described.[21] Briefly, fibroin protein was completely solubilized in 1M solution of LiCl
112 (Sigma Aldrich) in DMSO (99.9%, Fisher Scientific). After the addition of a stoichiometric
113 quantity of 2-isocyanoethyl methacrylate (IEM, Sigma Aldrich), the solution was maintained
114 under stirring for 5 hours at 60° C to allow the conjugation reaction. The entire procedure was
115 conducted in an anhydrous environment under continuous nitrogen flux. The solution was poured
116 into an excess of cold ethanol in order to precipitate the fibroin with methacrylate conjugated side
117 groups. The collected methacrylate protein was washed and centrifuged three times in a mixture
118 of 50% cold 200 proof ethanol (Koptec) and 50% acetone (Alfa Aesar). The final product (fibroin
119 protein photoresist (FPP)) was obtained after 48 hours of lyophilisation. In this work, the terms
120 FPP, fibroin, and photo-fibroin are used interchangeably as referring to the same material.[21]

121

122 **2.2. Surface treatment and functionalization**

123 Fibroin architectures were formed on silicon and glass substrates. To obtain a covalent adhesion
124 of the protein to the surface, functionalization with acrylate groups was required. A bath of piranha
125 solution (3 parts 98% H_2SO_4:1 part 30% H_2O_2 (v/v)) was used to clean the substrates for 30
126 minutes in ambient condition (*Caution: Piranha solution is highly corrosive and reacts violently*
127 *with organic matter*). The functionalization with 3-(trichlorosilyl) propyl methacrylate (TPM,
128 Sigma Aldrich) was conducted using a chemical vapor deposition in a vacuum dryer for 12 hours
129 at 0.4 bars. Surfaces were subsequently washed with methanol (Fisher Scientific) and water in
130 order to remove any excess TPM.

131

132 **2.3. Film fabrication**

133 Films were prepared starting from a 5% (w/v) solution of FPP in formic acid (FA, Acros Organics
134 98%) or in 1,1,1,3,3,3-hexafluoro-2-propanol (HFIP, Oakwood Chemicals). The samples were
135 prepared by casting the solutions on silicon substrates or using a spin coating process (SPS spin
136 150). An angular velocity ranging from 1000-4000 rpm was used (maintaining the other condition
137 fixed such as angular acceleration: 200 rpm/s^2, duration: 60 s). To produce thinner films suitable
138 for ellipsometric measurement (thickness and refractive index), the concentration was reduced to
139 1.5% and 1.2% w/v. In this case, the spin coating process (2000 rpm, 100 rpm/s^2, 60 s) was
140 conducted on TPM treated silicon surface.

141

142 **2.4. Photolithographic process**

143 A microscale test pattern was fabricated using contact lithography. A photoinitiator (Irgacure
144 2959, BASF) 1.6% (w/v) was added to the FPP/FA 5% solution and mixed. Spin coating was
145 conducted on functionalized silicon or glass surfaces. The obtained films were stored for a few
146 hours in a fume hood to achieve complete evaporation of the solvent. Films were also fabricated
147 via an accelerated drying process using a hot plate at 50° C with a temperature ramp of 10° C/15
148 minutes to room temperature (1 hour to complete the process). The cooling ramp allows rapid
149 formation of a dry film without temperature-induced shrinkage. The obtained films were exposed
150 through a photomask for 2 seconds at 2 mW/cm^2 at 365 nm (Lumen Dynamics OmniCure 1000),
151 developed in a 1M DMSO/LiCl solution for 2 hours, and washed with a large amount of water.

152 **2.5. Film Characterization**

153 Thickness profiles were measured using a Veeco Dektak 150 Stylus Profilometer, with the mean
154 and standard deviation calculated over different areas on each film. Asylum MFP-3D atomic force
155 microscope (AFM) and Zygo New View 6300 optical profilometer were used to analyze film

156 morphology and surface roughness. Imaging was conducted using a Nikon Eclipse LV100D
157 optical microscope and a JEOL LV-5610 SEM instrument. The measurement of thickness for the
158 thinner films was obtained using a SENTECH SE800 Spectroscopic Ellipsometer. Refractive
159 index was obtained by fitting two contemporary spectra at 60° and 70° using a Cauchy absorbance
160 model (Horiba UVISEL 460). Transmittance and absorbance measurements were conducted using
161 a JASCO VR-570 UV-Vis spectrophotometer. Secondary structures were determined by Fourier
162 transform infrared spectroscopy (FTIR) in attenuated total reflectance mode (ATR) (Perkin-Elmer
163 Spectrum One spectrophotometer equipped with Zinc Selenide crystal). High resolution spectra
164 were obtained at one point/cm^{-1}, averaging 8 spectra for each sample to reduce the noise. Thermal
165 analysis was conducted in a range of 30-330° C using a differential scanning calorimeter (Mettler-
166 Toledo DSC 20) in nitrogen atmosphere with a heating rate of **10° C**/min. Thermal gravimetric
167 analysis (TGA) (Mettler-Toledo TG50 thermobalance) was conducted over 35-450° C in nitrogen
168 atmosphere with a heating rate of 10° K/min.
169

170 **3. Results and Discussion**

171

172 Thin films are of outstanding interest for applications such as electronics, development of MEMS
173 components, microfluidic devices, and substrate coatings. While films may be formed by solvent
174 casting, one of the most scalable and easy techniques to form uniform films on substrates is via
175 spin coating. This process is widely used for commercial photoresists, and has been extensively
176 used for the deposition of aqueous solutions of fibroin (e.g., regenerated silk fibroin (rSF)
177 solubilized using LiBr).[26] However, this has not been suitable for forming thin (100-1000 nm) and
178 ultrathin (1-100 nm) silk films. Aqueous solutions of fibroin are not particularly suitable for spin
179 coating, or high resolution patterning applications at the micro and nanoscales. For optical

180 applications, thin films of optical quality with minimal defects are highly desired. In such cases,
181 HFIP as solvent has been widely used. However, HFIP comes with a host of issues that make the
182 development of alternative solvents very attractive. The choice of the solvent is further
183 fundamental to the process of spin coating itself, as it affects the viscosity of the film and coating
184 parameters. In this study, we show how photocrosslinkable fibroin using FA as the solvent,
185 coupled with the technique of spin coating allows the formation of films of controllable thickness.
186 The films are formed with excellent surface qualities. The possibility of forming precise patterns
187 and structures can extend the use of this system over the common use of photoresists or regular
188 (unmodified) fibroin (viz. rSF) for various applications.
189

190 **3.1. Spin coating of nanoscale films**

191 FA and HFIP solutions of photo-fibroin at the same concentration (5% w/v) were used to produce
192 films via spin coating using identical process conditions. To observe the effect of chuck speed on
193 film thickness, the maximum achieved rotations per minute (RPM) were set to 1000, 1500, 2000,
194 3000, 4000 with an angular acceleration of 200 rpm/s^2 for 60 seconds. On each film six thickness
195 values were measured at different locations to obtain a mean and standard deviation. The results
196 are shown in **Figure 1**. As may be observed, the use of FA as a solvent formed thinner and more
197 homogeneous films in comparison to the films produced under the same conditions using HFIP as
198 solvent (**Figure 1a**). The mean thickness of HFIP films are typically 2-4 times the thickness of FA
199 films formed under the same conditions (**Figure 1a**). The uniformity of film is proportional to the
200 mean thickness standard deviation (**Figure 1b**). This measure was calculated to quantitatively
201 determine the variance of height across different films prepared under similar conditions. The
202 higher standard deviation using HFIP shows that that the reproducibility of film thickness with FA
203 was higher. At ~3000 rpm, thin films (0.54±0.02 μm thickness) were formed with a very low

204 deviation. To form thinner films, the concentration of the solution was reduced. Using a
205 concentration of 1.5% w/v in FA, we obtained films with a thickness of ~172 nm, and using a
206 concentration of 1.2% w/v, a thickness of ~115 nm could be consistently obtained at process
207 parameters of 2000 rpm (max speed), 100 rpm/s, 30 s (angular acceleration). The film thickness
208 was confirmed via ellipsometry (**Figure 1c, d**).
209

210 **3.2. Optical characterization of nanoscale films**

211 Films using FA tend to have a higher uniformity of thickness regardless of the spin coating
212 conditions. We may hypothesize that this effect is related to the lower evaporation rate of the
213 solvent, which allows a better control over the spin coating process and a longer time for achieving
214 a stable configuration. The uniformity of the FA films can be clearly noticed comparing the films
215 made by the two different solvents (**Figure 2a**). Indeed, the standard deviation for the HFIP films
216 is on the order of hundreds of nanometers so that the film features are large enough to be seen by
217 the naked eye (**Figure 2b**). In contrast, thin, optical grade films of fibroin can therefore be easily
218 obtained using spin casting process in combination with a solution in FA with a low concentration.
219

220 The transmittance of the films was measured using a UV-Vis spectrophotometer (**Figure 2c**). Over
221 the visible range (400nm-700nm), FA fibroin films tend to have flat spectra with transmittance
222 around 90%. In comparison, the films made with HFIP are not flat and their transmittance
223 monotonically decreases from 68% (700 nm) to 45% (400 nm). Absorbance spectra show the UV
224 absorption edge of both films, lying around 300 nm. No other bands indicating yellowing o
225 oxidation processes are present. The flat and high transmittance spectra ensure that fibroin films
226 made by FA are transparent and colorless. In contrast, the lower transmittance spectra of the HFIP
227 films is indicative of low transparency due to the scattering from the surface roughness evidenced

228 by the profilometry measurements discussed belowThe observed high transmittance over the
229 visible spectrum represents a potential issue in optical applications, where the light needs to be
230 transmitted inside the material. So, formic acid is preferable over HFIP as a solvent of choice for
231 fibroin for optical applications such as low loss waveguides.
232
233 Interestingly,the high optical quality of these films allowed ellipsometric analysis, which is quite
234 unusual in case of protein materials due the their typical optical inhomogeneity. Solutions of
235 fibroin in FA tend to have low turbidity even in comparison to solutions in water.[23]Since the
236 electrical repulsion of the positively charged fibroin molecules in acid solution prevents
237 coagulation. On the other hand, fibroin molecules tend to aggregate in water due to hydrophobic
238 interactions.[23] Indeed, the hydrodynamic radius (R_H) calculated using Dynamic Light Scattering
239 (DLS) shows an average radius of 19 nm in FA and 139 nm in water.[24] The refractive index (RI)
240 of FA films was investigated. The value is observed to increase monotonically from 1.55 (900 nm)
241 to 1.58 (450 nm). The slightly higher value of RI at 630 nm (1.56) than the value reported in
242 literature for films of rSF (1.54) is likely due to the introduction of methacrylate groups as
243 discussed above.[35, 36] These results suggest that FA is a better choice for optical applications
244
245 **3.3. Film characterization using AFM morphology and profilometry**
246 The films were characterized using various techniques to study the surface properties at the
247 nanoscale. A comparison between film morphologies using atomic force microscopy (AFM)
248 shows no significant difference between films made by HFIP and FA at the nanoscale (**Figure 3**).
249 The root mean square (RMS) roughness in both case is ~5 nm over a 25 μm^2 area. Nanoscale holes
250 are present in both sets of films as previously observed on rSF.[37] What is also interesting is that a
251 similar nanoscale morphology appears regardless of the method of film fabrication – casting vs.

spin coating. In these experiments, cast films were typically thick (on the order of several μm).

On the other hand, over larger areas, FA films are observed to be flatter than HFIP films. Optical profilometry over a rectangular surface of 1.424 mm^2 shows a roughness of 57 nm for FA films in comparison to 327 nm for HFIP films (**Figure 4a, b**). This seeming discrepancy in roughness values in comparing small areas (25 μm^2) to larger areas (5 mm) may be easily understood by the ~5 orders of magnitude difference from the micro to the millimeter scale. A similar result is obtained by line profilometry (**Figure 4c**) with roughness value of 13 nm for FA films and 179 nm for HFIP films. Both methods validate the lower roughness and more uniform nature of films made by FA solution, which further ensures low surface scattering. The lower roughness of FA films at the microscale can be explained considering the effect of the carboxyl group on the fibroin conformation and the lower volatility of FA.[24]

3.4. Secondary structure characterization

The primary amide peak was used to evaluate the secondary structure content in FPP films made using each solvent. Peaks related to the different secondary structures [38, 39] were fit inside the primary amine peak and, another peak centered at 1725 cm^{-1} was fit to account for the presence of methacrylate side groups introduced due to chemical functionalization.[21] **Figure 5** shows the IR spectra (black line), the fitted peaks (green line), and the fitted curve (red line). Fitting was performed using Voigt peaks and minimizing the χ^2 function, to calculate the percentage of content of each structure. The quantitative data is reported in **Table 1**. Per this analysis, films formed using FA display a higher content of β-sheet (38.0%), and lower content of random coil (18.7%), α-helices (6.5%) and turns (16.6%) in comparison with films prepared using HFIP for which the content of each structure is 22.6%, 36.5%, 13.0% and 23.2% respectively. This is not unexpected

276 as FA has been reported to promote the formation of β-sheets via a conformational change from
277 random coils in a variety of protein systems including fibroin and keratin.[24, 40] The greater content
278 of β-sheets in FA films may decrease its transparency due to the presence of crystallites inside the
279 amorphous structure that act as scattering centres. This effect is less important than the surface
280 effect; in fact, the highest difference in the refractive index between air and the bulk material
281 respect to crystalline and amorphous part of the bulk gives a higher scattering on the surface than
282 inside the bulk.[41] For these reasons, despite the higher content in ordered structure, FA films result
283 to have a higher transmittance than HFIP films.
284

285 **3.5. Thermal analysis**

286 DSC curves for both films are shown in **Figure 6a.** The first wide endothermic peak is present for
287 both films, and indicates the evaporation of bonded water.[30, 39, 42] In particular, for FA this peak is
288 centred at 100°C (ΔH=35.6 $J.g^{-1}$) whereas for HFIP, this peak is centred at 75°C (ΔH=42.8 $J.g^{-1}$).
289 An exothermic peak of crystallization (160.4°C, ΔH=4.8 $J.g^{-1}$) is present only for HFIP, and can
290 be related to the random coil–β-sheet transition. The lower temperature of this transition with
291 respect to earlier reported values,[30, 39, 42] is probably related to the presence of the functionalization
292 groups that promotes the formation of β-sheet structures. Indeed, the absence of this peak in FA
293 confirms that the β-sheet formation occurs due to drying from FA solution.[24] The degradation peak
294 is centred at 271° C (ΔH=99.1 $J.g^{-1}$) with a shoulder centred at 282°C in case of HFIP, and 281°
295 C (ΔH=50.1 $J.g^{-1}$) in case of FA. The peak at 271° C could be related to degradation of insoluble
296 helixes, [39] while the peak at 281° C to the degradation of the more stable β-sheets. The glass
297 transition temperature (T_g) is also different and can be detected at 150° C and 158° C respectively
298 for HFIP and FA. TGA curves shows an initial weight loss due to water evaporation (35-170° C
299 for HFIP, 35-135° C for FA), the higher weight loss of the sample prepared using HFIP (9% versus

300 4% of FA film) is consistent with its higher amount of amorphous phase. The evaporation of other
301 low temperature volatile components give the second weight loss (170° C-280° C weight loss
302 29.0% for HFIP, 135-300° C weight loss of 19.5% for FA).[30] At higher temperatures the fibroin
303 decomposition begins; the higher amount of remaining mass for FA (74%) vs. HFIP (66%) at the
304 start of the decomposition and, the lower slope in the decomposition region (maximum slope
305 0.0058 mg.°C^{-1} for FA vs. 0.0074 mg.°C^{-1} for HFIP) collectively demonstrate the better thermal
306 stability of films made by FA.
307

308 **3.6. Micropatterning of fibroin using formic acid as a solvent**

309 As discussed above, in this work, the biochemically modified photo-crosslinkable fibroin was used
310 for the film fabrication. As shown before by our group, this variant of fibroin is very similar in
311 properties to rSF but allows the precise patterning of microscale architectures using UV light
312 assisted photolithography,[21] wherein the material behaves as a negative tone photoresist. However,
313 in the prior work, the patterning was conducted using HFIP as solvent (Note: because of previous
314 reports by our group showing these results,[21, 43] the patterning is not shown here). Using FA as a
315 solvent does not alter the ability to form microscale architectures of similar resolution and fidelity
316 using photolithography. Films fabricated as discussed above were exposed to 365 nm UV light
317 through a chrome photomask via contact photolithography. Following development of the films to
318 remove the un-crosslinked material, the structures are attached to the underlying substrate
319 (typically silicon or glass). **Figure 7** shows the structures that can be formed via this process.
320 Microstructures with a dimension of 3-100 μm can be easily obtained over large areas with high
321 precision. As a high throughput technique, this method can be used to form large areas of precise
322 fibroin micropatterns. AFM imaging shows the high resolution lines that can be formed (**Figure**
323 **7b**). Line profiles of the patterns using AFM reveal a thickness of 100 nm, which is consistent with

ellipsometric measurements that gives a result of 115 nm (note that the ellipsometry values are for films). Close up of the patterns shows smooth, uniform features with a surface roughness of 8.1 nm over 5 μm square area (**Figure 7c**). Thus, FA is a viable solvent for the process of silk lithography with high resolution architectures and controllable aspect ratios.

4. Conclusions

In summary, photocrosslinkable fibroin was successfully dissolved in FA as an alternative solvent to the conventionally used solvent HFIP. This vastly reduces the cost and the environmental impact of using fibroin for various applications. The lower evaporation rate allows for better control of the deposition process giving rise to robust, uniform films. Films that are up to four times thinner than those formed using HFIP can be fabricated. This makes the technique suitable for the production of thin and ultrathin films, below 100 nm by optimizing various parameters such as concentration of the precursor solution and spin coating speed. Morphological and optical analyses show how these films provide significant improvements in flatness and optical transparency. Structural analysis reveal differences in β-sheet content of the two films and the higher thermal stability of FA films. Importantly, due to the ability to form micropatterns with this material, high-resolution patterning is demonstrated, opening the possibility of the use of silk fibroin in applications that requires features with a smooth and uniform surface such as optical biosensors and bioelectronics. Further studies are ongoing for the determination of the optical constants and refractive indices of these new types of optical films and microstructures.

References

1. L.-D. Koh, Y. Cheng, C.-P. Teng, Y.-W. Khin, X.-J. Loh, S.-Y. Tee, M. Low, E. Ye, H.-D. Yu, Y.-W. Zhang and M.-Y. Han, *Progress in Polymer Science*, 2015, **46**, 86-110.
2. B. Kundu, N. E. Kurland, S. Bano, C. Patra, F. B. Engel, V. K. Yadavalli and S. C. Kundu, *Prog Polym Sci*, 2014, **39**, 251-267.
3. C. Vepari and D. L. Kaplan, *Prog Polym Sci*, 2007, **32**, 991-1007.
4. Q. Zhang, S. Yan and M. Li, *Materials*, 2009, **2**, 2276-2295.
5. Q. Zhang, S.-Q. Yan and M.-Z. Li, *Journal of Fiber Bioengineering and Informatics*, 2010, **3**, 1-8.
6. R. K. Pal, A. A. Farghaly, M. M. Collinson, S. C. Kundu and V. K. Yadavalli, *Advanced materials*, 2016, **28**, 1406-1412.
7. B. Zhu, H. Wang, W. R. Leow, Y. Cai, X. J. Loh, M. Y. Han and X. Chen, *Advanced materials*, 2016, **28**, 4250-4265.
8. D. S. Lu, Z. Z. Zheng, S. Z. Guo, C. Wang, D. L. Kaplan and X. Q. Wang, *J. Sens.*, 2015, DOI: 10.1155/2015/819373, 10.
9. J. MacLeod and F. Rosei, *Nature materials*, 2013, **12**, 98-100.
10. N. C. Tansil, L. D. Koh and M. Y. Han, *Advanced materials*, 2012, **24**, 1388-1397.
11. S. A. Bhakta, E. Evans, T. E. Benavidez and C. D. Garcia, *Analytica chimica acta*, 2015, **872**, 7-25.
12. A. K. Yetisen, H. Butt, L. R. Volpatti, I. Pavlichenko, M. Humar, S. J. Kwok, H. Koo, K. S. Kim, I. Naydenova, A. Khademhosseini, S. K. Hahn and S. H. Yun, *Biotechnology advances*, 2016, **34**, 250-271.
13. H. Tao, D. L. Kaplan and F. G. Omenetto, *Advanced Materials*, 2012, **24**, 2824-2837.

368 14. J. J. Amsden, P. Domachuk, A. Gopinath, R. D. White, L. Dal Negro, D. L. Kaplan and F.
369 G. Omenetto, *Advanced Materials*, 2010, **22**, 1746-+.
370 15. H. Perry, A. Gopinath, D. L. Kaplan, L. Dal Negro and F. G. Omenetto, *Advanced*
371 *materials*, 2008, **20**, 3070-3072.
372 16. K. Tsioris, H. Tao, M. Liu, J. A. Hopwood, D. L. Kaplan, R. D. Averitt and F. G. Omenetto,
373 *Advanced materials*, 2011, **23**, 2015-2019.
374 17. S. Kim, B. Marelli, M. A. Brenckle, A. N. Mitropoulos, E. S. Gil, K. Tsioris, H. Tao, D. L.
375 Kaplan and F. G. Omenetto, *Nature nanotechnology*, 2014, **9**, 306-310.
376 18. F. Galeotti, A. Andicsova, S. Yunus and C. Botta, *Soft matter*, 2012, **8**, 4815.
377 19. Y. Tsuboi, H. Adachi, K. Yamada, H. Miyasaka and A. Itaya, *Japanese Journal of Applied*
378 *Physics*, 2002, **41**, 4772-4779.
379 20. M. B. Applegate, B. P. Partlow, J. Coburn, B. Marelli, C. Pirie, R. Pineda, D. L. Kaplan
380 and F. G. Omenetto, *Advanced materials*, 2016, **28**, 2417-2420.
381 21. N. E. Kurland, T. Dey, S. C. Kundu and V. K. Yadavalli, *Advanced Materials*, 2013, **25**,
382 6207-6212.
383 22. E. S. Sashina, A. M. Bochek, N. P. Novoselov and D. A. Kirichenko, *Russian Journal of*
384 *Applied Chemistry*, 2006, **79**, 869-876.
385 23. I. C. Um, H. Y. Kweon, Y. H. Park and S. Hudson, *International journal of biological*
386 *macromolecules*, 2001, **29**, 91-97.
387 24. I. C. Um, H. Y. Kweon, K. G. Lee and Y. H. Park, *International journal of biological*
388 *macromolecules*, 2003, **33**, 203-213.
389 25. S. W. Ha, A. E. Tonelli and S. M. Hudson, *Biomacromolecules*, 2005, **6**, 1722-1731.

390 26. D. N. Rockwood, R. C. Preda, T. Yucel, X. Q. Wang, M. L. Lovett and D. L. Kaplan,
391 *Nature Protocols*, 2011, **6**, 1612-1631.
392 27. H. J. Jin, S. V. Fridrikh, G. C. Rutledge and D. L. Kaplan, *Biomacromolecules*, 2002, **3**,
393 1233-1239.
394 28. R. Pohanish, *HANDBOOK OF TOXIC AND HAZARDOUS CHEMICALS AND*
395 *CARCINOGENS*, William Andrew, 6 edn., 2011.
396 29. X. X. Yue, F. Zhang, H. Y. Wu, J. F. Ming, Z. H. Fan and B. Q. Zuo, *Materials Letters*,
397 2014, **128**, 175-178.
398 30. A. Motta, L. Fambri and C. Migliaresi, *Macromol Chem Physic*, 2002, **203**, 1658-1665.
399 31. C. Y. Jiang, X. Y. Wang, R. Gunawidjaja, Y. H. Lin, M. K. Gupta, D. L. Kaplan, R. R.
400 Naik and V. V. Tsukruk, *Adv Funct Mater*, 2007, **17**, 2229-2237.
401 32. D. Meyerhofer, *Journal of Applied Physics*, 1978, **49**, 3993.
402 33. X. Wang, X. Hu, A. Daley, O. Rabotyagova, P. Cebe and D. L. Kaplan, *Journal of*
403 *controlled release : official journal of the Controlled Release Society*, 2007, **121**, 190-199.
404 34. S. Ling, K. Jin, D. L. Kaplan and M. J. Buehler, *Nano letters*, 2016, **16**, 3795-3800.
405 35. S. T. Parker, P. Domachuk, J. Amsden, J. Bressner, J. A. Lewis, D. L. Kaplan and F. G.
406 Omenetto, *Advanced materials*, 2009, **21**, 2411-2415.
407 36. M. B. Applegate, G. Perotto, D. L. Kaplan and F. G. Omenetto, *Biomedical optics express*,
408 2015, **6**, 4221-4227.
409 37. B. Kundu, N. E. Kurland, V. K. Yadavalli and S. C. Kundu, *Int J Biol Macromol*, 2014,
410 **70**, 70-77.
411 38. X. Hu, D. Kaplan and P. Cebe, *Macromolecules*, 2006, **39**, 6161-6170.

412 39. E. Callone, S. Dire, X. Hu and A. Motta, *Acs Biomaterials Science & Engineering*, 2016,
413 **2**, 758-767.
414 40. A. Vasconcelos, G. Freddi and A. Cavaco-Paulo, *Biomacromolecules*, 2008, **9**, 1299-1305.
415 41. R. Pritchard, *Polymer Engineering & Science*, 1964, **4**, 66-71.
416 42. M. Tsukada, Y. Gotoh, M. Nagura, N. Minoura, N. Kasai and G. Freddi, *J Polym Sci Pol*
417 *Phys*, 1994, **32**, 961-968.
418 43. R. K. Pal, N. E. Kurland, C. Wang, S. C. Kundu and V. K. Yadavalli, *Acs Appl Mater Inter*,
419 2015, **7**, 8809-8816.

420

Solvent	HFIP		FA	
Structure	**Peak position (cm^{-1})**	**% Area**	**Peak position (cm^{-1})**	**% Area**
Side chain	1610	**4.8**	1610	**16.2**
β-sheet	1619 1624 1630 1700	3.3 1.0 16.6 1.7	1619 1624 1630 1700	13.2 8.6 11.2 5.0
Total		**22.6**		**38.0**
Random coil	1642 1651	20.5 16.0	1642 1651	11.7 7.0
Total		**36.5**		**18.7**
α-helices	1659	**13**	1659	**6.5**
Turns	1667 1678 1691	10.5 9.5 3.2	1667 1678 1691	4.5 11.5 0.9
Total		**23.2**		**16.6**

Table 1: Quantitative data and peak assignments of the fitted peaks in the Amide I IR band for the two solvents, HFIP and FA.

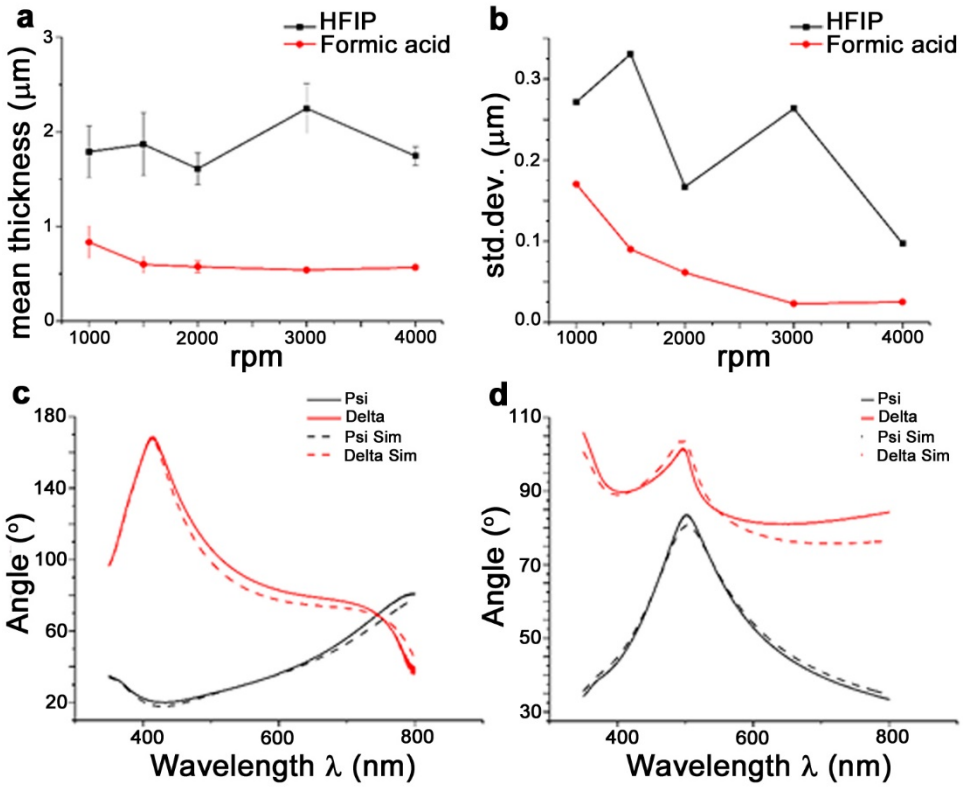

Figure 1: Film thickness data for fibroin films formed by spin coating of solution made with two different solvents - HFIP (black) and FA (red): (a) mean thickness trend over rpm, (b) standard deviation of the mean thickness trend over rpm. (c, d) Ellipsometry spectra for thickness determination of thin fibroin films made by spin coating of low concentration solutions in FA: (c) 1.7% w/v, (d) 1.2% w/v. (Psi (blue) and Delta (red) measured (solid line) and simulated (dashed line).

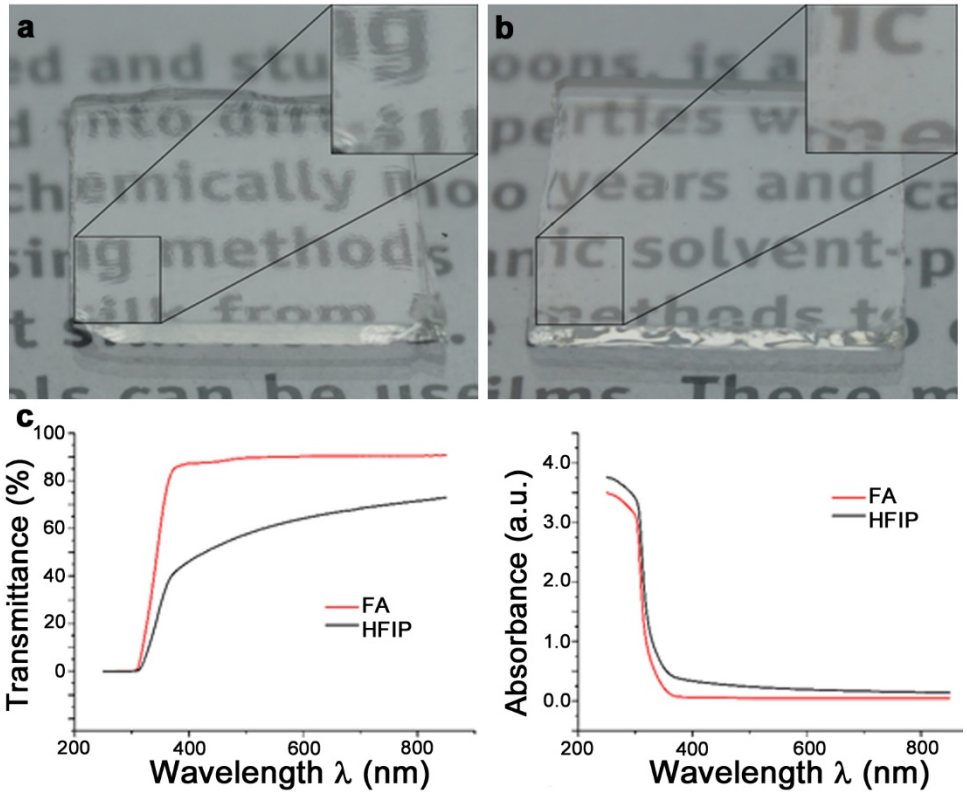

Figure 2: Images of films obtained by solvent casting showing optical properties: produced using (a) HFIP (b) FA. (c) UV-Vis spectra of films made using FA (red) and HFIP (black) showing the percentage transmittance and absorbance spectra.

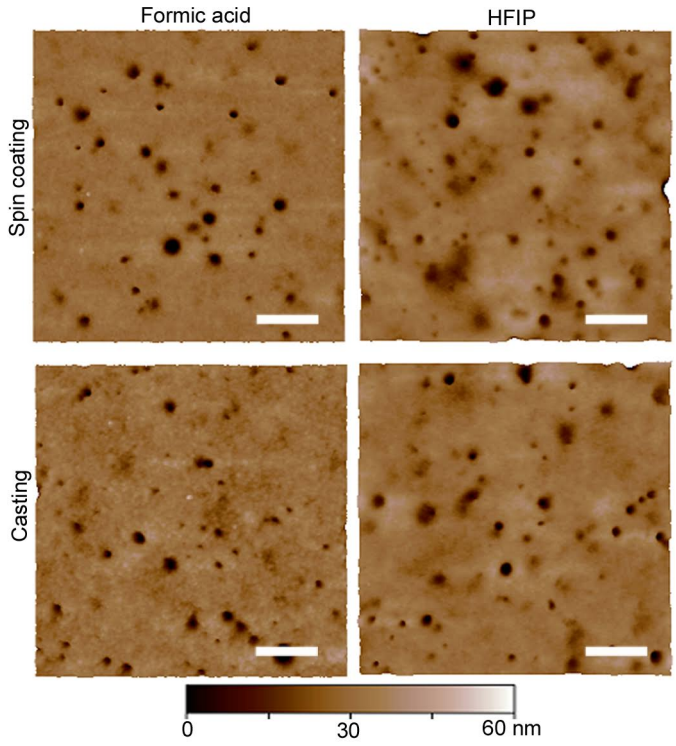

Figure 3: AFM images of films produced using different methods (Spin coating on the top, Film casting on the bottom) and different solvent ((L) FA, (R) HFIP). Scale bar=1 µm.

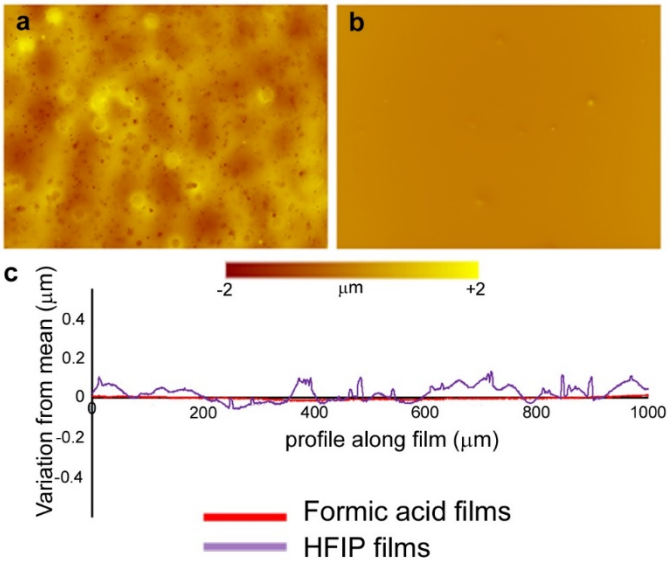

Figure 4: Optical profilometry images of films produced by casting on a glass substrate using: (a) HFIP, (b) FA. (c) Mean value of 5 line profiles performed over films made by the two solvents (FA (red), HFIP (purple)).

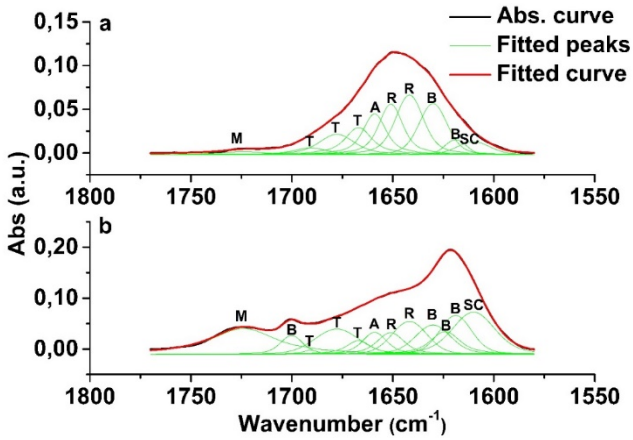

470

471 **Figure 5:** FTIR-ATR spectra of the primary amide peaks of films produced using (a) HFIP (b)

472 FA. The peak fits (green) relate to the different secondary structures and side groups (SC: side

473 chain; B: β sheets, R: random coil, A: α-helix, T: turns; M: methacrylate group).

474

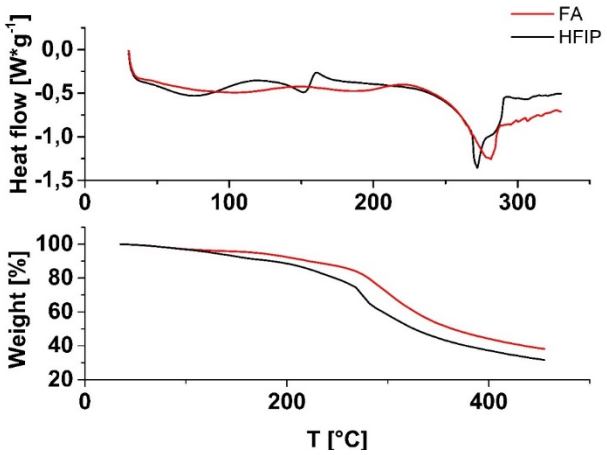

Figure 6: (a) DSC and (b) TGA curves for films made using FA (red) and HFIP (black).

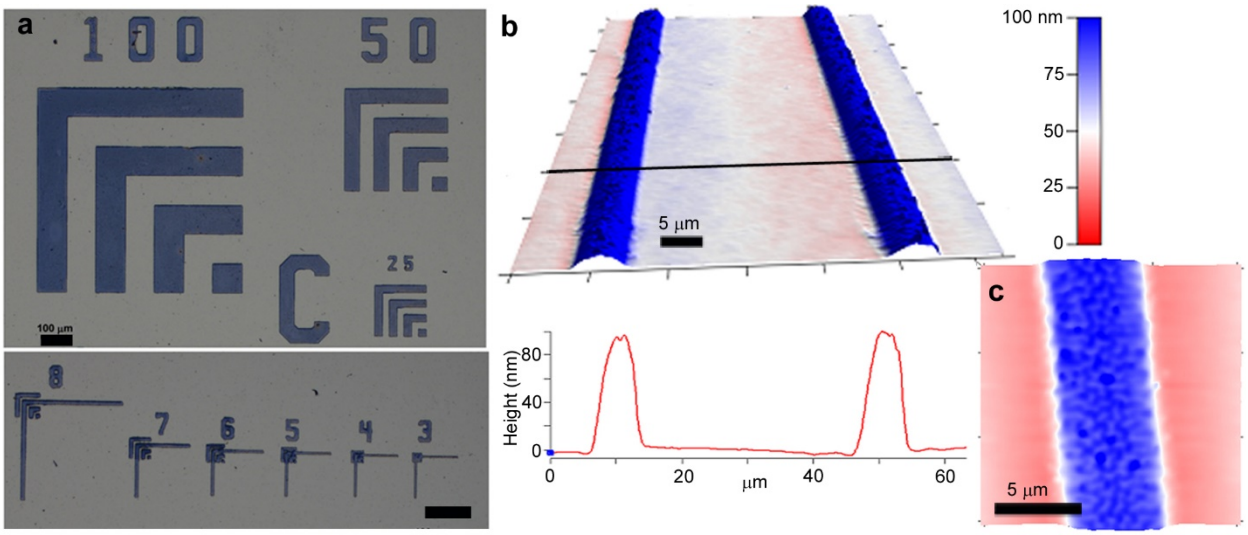

Figure 7: (a) Optical microscopy images of fibroin micropatterns formed on a silicon surface using photolithography with FA as solvent. Coomassie brilliant blue was used to stain the patterns for easy visualization (scale bar = 100 µm). (b) AFM image of nanoscale thin films patterned with 5 µm lines. The line profile below shows that the feature height is ~100 nm. (c) Close-up of the lines shows the uniformity of the micropatterns (scale bar = 5 µm).